

Cooper minima in the transitions from low-excited and Rydberg states of alkali-metal atoms

I. I. Beterov,^{1,*} C. W. Mansell,² E. A. Yakshina,¹ I. I. Ryabtsev,¹ D. B. Tretyakov,¹
V. M. Entin,¹ C. MacCormick,² M. J. Piotrowicz,^{2,3} A. Kowalczyk,² and S. Bergamini²

¹*A.V.Rzhanov Institute of Semiconductor Physics SB RAS,
Prospekt Lavrentieva 13, 630090 Novosibirsk, Russia*

²*The Open University, Walton Hall, MK7 6AA, Milton Keynes, UK*

³*University of Wisconsin-Madison, 1150 University Avenue, Madison, Wisconsin 53706, USA*

(Dated: 12 July 2012)

The structure of the Cooper minima in the transition probabilities and photoionization cross-sections for low-excited and Rydberg nS , nP , nD and nF states of alkali-metal atoms has been studied using a Coulomb approximation and a quasiclassical model. The range of applicability of the quasiclassical model has been defined from comparison with available experimental and theoretical data on dipole moments, oscillator strengths, and photoionization cross-sections. A new Cooper minimum for transitions between rubidium Rydberg states has been found.

PACS numbers: 32.80.Ee, 03.67.Lx, 34.10.+x, 32.70.Jz, 32.80.Rm

I. INTRODUCTION

Spectral line series of alkali metal atoms display remarkable features with prominent minima in the transition probabilities, emission oscillator strengths or photoionization cross-sections [1–13]. These minima arise from the cancellation of the radial integral for some transitions, depending on the overlap between the wavefunctions of the initial and final quantum states of the atoms [1, 2], and are well known as Cooper minima [3, 4].

Observation of the Cooper minima in the photoionization cross-sections and in the transition probabilities of the discrete spectrum provides valuable information about the electronic structure of the atoms. Minima in photoionization cross sections were first found experimentally in Ref. [5] and explained 20 years later by Cooper [3]. The sharp minima in the emission probabilities for some Rydberg states of alkali-metal atoms were first discussed by Theodosiou [6].

The experimental investigation of Cooper minima can be used for the verification of theoretical calculations of spectroscopic properties of atoms and molecules. For example, experimentally measured photoionization cross-sections for sodium ground state showing the Cooper minimum [7], were in good agreement with the theoretical calculations of Aymar [8], which confirmed the accuracy of the theoretical model.

Cooper minima in the discrete spectrum are revealed as a suppression of the two-photon photoionization [10] or sharp decrease of the emission oscillator strengths [6]. The map of these minima could be valuable for systematic studies of the processes which involve a large number of transitions, such as calculation of lifetimes of Rydberg atoms [14], blackbody-radiation-induced photoionization

rates [15, 16] or collisional ionization cross-sections of cold atoms [17].

Photoionization of alkali-metal atoms recently attracted a lot of interest, as it has taken a central role in experiments with cold atoms in far-off-resonance traps [18, 19], in photoionization spectroscopy [20–22], measurement of oscillator strengths [21–23], photoionization cross-sections and lifetimes of excited atoms [14, 21–29], and photoionization of the Bose-Einstein condensate [30, 31].

Rydberg atoms with large principal quantum numbers $n \sim 50$ –100 recently received attention due to the progress achieved in experiments with cold atomic samples. These samples are often prepared in optical traps whose intense laser field could make the ionization lifetimes of Rydberg atoms extremely short. However, for certain wavelengths, ionization rates could be significantly reduced due to Cooper minima in the photoionization cross-sections [3]. Therefore it would be most useful to exploit trapping schemes operated at wavelengths displaying Cooper minima to avoid photoionization [18, 32].

In this paper we have calculated the radial matrix elements of arbitrary bound-bound, bound-free and free-free transitions between S , P , D and F states of alkali-metal atoms using the quasiclassical model by Dyachkov and Pankratov (DP model) [33, 34]. In section II we present examples of the Cooper minima for bound-free and bound-bound transitions and discuss the accuracy of the theoretical method. Numerical results are presented in Section III as density plots, revealing the Cooper minima in bound-bound, bound-free and free-free transitions.

* beterov@isp.nsc.ru

II. THE QUASICLASSICAL MODEL AND ITS APPLICABILITY

Radial matrix elements of the electric dipole transitions between arbitrary atomic states (e.g., bound-bound or bound-free transitions) are required to calculate the spectroscopic properties of atoms, including oscillator strengths, lifetimes, photoionization cross-sections, and rates of collisional ionization.

Although alkali-metal atoms have a single valence electron, only states with small quantum defects exhibit truly hydrogen-like behavior. Due to non-hydrogenic character of alkali-metal atoms, the calculation of radial matrix elements remains a challenging task, since no exact analytical solution for arbitrary transitions is available yet [35]. The oscillator strengths for alkali-metal atoms can strongly deviate from the values for hydrogen. Accurate calculation of the radial integral for transitions between states with small angular momentum are difficult because of the need to take into account the interaction of the valence electron with the atomic core.

A method based on the Coulomb approximation relies on the idea that the Rydberg electron is localized mostly outside the atomic core, where the potential is Coulombic. In the Numeric Coulomb Approximation [36] the radial wavefunctions are obtained by solution of the Shrodinger equation with the exact energies of the alkali-metal quantum states, expressed through the quantum defect (Rydberg-Ritz formula, atomic units are used in this paper):

$$E_n = -\frac{1}{2n_{eff}^2}. \quad (1)$$

Here $n_{eff} = n - \mu_L$ is an effective quantum number, μ_L is the quantum defect. Quantum defect accounts for the penetration of the valence electron into the ionic core of a Rydberg atom. The quantum defects are used as input parameter for the calculations and the integration is truncated at the inner core radius.

Alternative forms of the Coulomb approximation were developed in [37]. The Modified Coulomb Approximation (MCA) is a generalization of the analytical expression for the hydrogen radial integral for non-integer quantum numbers. It allows direct calculation of the radial matrix elements without numeric integration.

Further simplification of the calculations in the Coulomb approximation is achieved by extension of the quasiclassical approximation to the states with low principal quantum numbers [33, 34]. The radial matrix elements are expressed through transcendental functions, which help to avoid inaccurateness of the direct numerical integration. This method can substantially improve both the speed and reliability of the calculations. However, the validity of most quasiclassical models was restricted by transitions between neighboring excited states [38–42].

In our previous works [14, 16] we used the quasiclassical model developed by Dyachkov and Pankratov [33, 34].

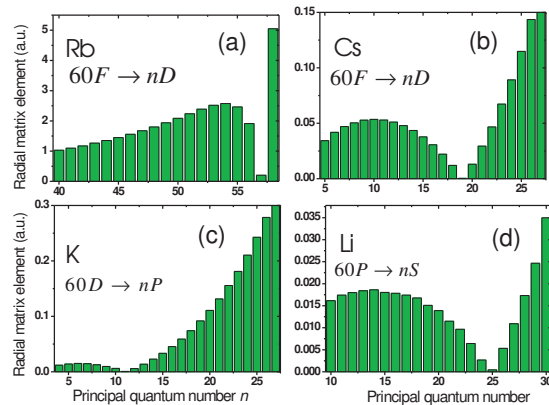


FIG. 1. (Color online). The calculated radial matrix elements for bound-bound (a) $60F \rightarrow nD$ transitions in rubidium; (b) $60F \rightarrow nD$ transitions in cesium; (c) $60D \rightarrow nP$ transitions in potassium; (d) $60P \rightarrow nS$ transitions in lithium.

Their original approach provides more precise values for the wave functions of the Rydberg and continuum states, compared to the other quasiclassical models. Good agreement with numeric results based on NCA model [36] or various model potential methods [43, 44] is observed.

Radial matrix elements for transitions between excited states of alkali-metal atoms display numerous features in their dependencies on n . For example, minima were revealed in the transition probabilities for $nD \rightarrow n'F$ in cesium [6] and for $nD \rightarrow n'P$ in potassium. Hoogenraad et al. [10] observed theoretically and experimentally a Cooper minimum for $nS \rightarrow n'P$ transitions in lithium. To study the validity of the quasiclassical model for bound-bound transitions, we have calculated the transition probabilities for $nL \rightarrow n'L'$ transitions in alkali-metal atoms with $n < 100$ and $L, L' = 1, 2, 3$ using the DP quasiclassical model, which is depicted in Appendix B. Figure 1 shows the dependencies of the radial matrix elements on the principal quantum number n for $60F \rightarrow nD$ transitions in rubidium and cesium [Fig. 1(a) and Fig. 1(b), respectively], $60D \rightarrow nP$ transitions in potassium [Fig. 1(c)] and $60P \rightarrow nS$ transitions in lithium [Fig. 1(d)]. The observed minima for lithium, potassium and cesium are in agreement with the results of Refs. [6, 11]. The minima for $nF \rightarrow n'D$ transitions in rubidium appear only for high n , and have not been located yet, to the best of our knowledge. These minima lie in the microwave region of about 150 GHz and could be studied using microwave spectroscopy [45].

Direct measurement of the radial matrix elements is of great importance for verification of the theory. However, due to lack of available experimental data for transitions between excited states of alkali-metal atoms, new measurements are required. In order to benchmark the model, we have earlier measured the reduced matrix element for the diffuse series of rubidium [23].

We observed the Autler Townes splitting in a sam-

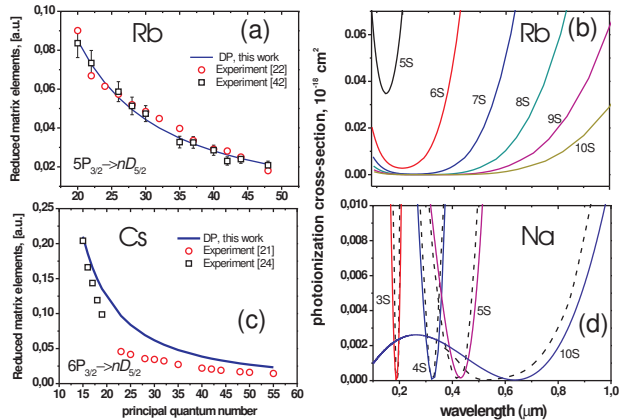


FIG. 2. (Color online). (a), (c) Comparison of the calculated reduced dipole moments for (a) rubidium atoms with experiment [22, 23] and (c) cesium atoms with experiment [21, 24]. (b), (d) Cooper minima in photoionization cross-sections of nS (b) rubidium and (d) sodium atoms. Solid curves - this work. Broken curves - theoretical calculations from Ref. [8];

ple of ultra-cold Rb atoms using a 3-level ladder system. Briefly, we monitored the absorption of a weak probe laser scanned over the $5S_{1/2} \rightarrow 5P_{3/2}$ whilst simultaneously a strong coupling laser, locked to the $5P_{3/2} \rightarrow nD_{5/2}$ transition illuminated the atoms. The strong coupling laser gave rise to two absorption peaks separated by the Rabi frequency of the atom-coupling laser interaction. Knowledge of the laser intensity allowed us to measure the dipole matrix elements of the $5P_{3/2} \rightarrow nD_{5/2}$ transitions to within 7% accuracy.

We have also compared the reduced dipole moments calculated using DP model with other available experimental data on diffuse series of rubidium [22, 23] and cesium [21, 24]. Good agreement with experiments of Refs. [22, 23] is confirmed in Fig. 2(a) for rubidium $5P \rightarrow nD$ transitions. For cesium the theoretical values in Fig. 2(c) are in agreement with the experiment only for the lowest nD states and differ from the experimental values for higher n by a factor of two. Our theoretical results for cesium are, however, in excellent agreement with the previous calculations of Ref. [24]. The observed disagreement between experiment and theory can result from improper account for core polarization for heavy cesium atoms [46]. However, we expect that for transitions between the states with larger principal quantum numbers the accuracy of the semiclassical approximation will be significantly increased due to smaller interaction of the Rydberg electron with the atomic core.

Calculated Cooper minima in the photoionization cross-sections of the nS states of rubidium and sodium are shown in Fig. 2(b) and (d), respectively. The solid curves in Fig. 2(b) and (d) represent the photoionization cross-sections calculated using our model based on the DP method. In the case of sodium, these are compared with the quantum-mechanical calculations of Ref. [8],

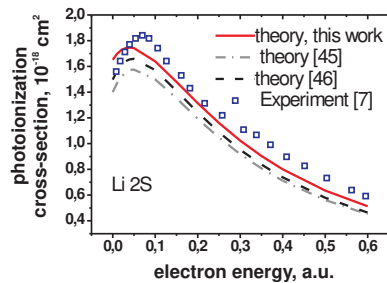


FIG. 3. (Color online). Lithium 2S photoionization cross-section. Comparison of the quasiclassical calculations with the experiment [7] and theory [47, 48].

shown as broken curves in Fig. 2(d). Good agreement is observed for sodium nS states with $n < 5$. For higher states the positions of the Cooper minimum are significantly shifted. In Ref. [49] it has been argued that the discrepancy in the quasiclassical calculations could be corrected by adjusting the phase in the radial integral in order to compensate the phase shift of the radial wavefunction from the value given by the quantum defect. At the same time, the reliability of the quasiclassical approximation is also expected to improve with the increase of the principal quantum number, and only experimental data could confirm the validity of the theory.

In figure 3 we have compared the calculated photoionization cross-section for lithium 2S state with the experiment of Ref. [7] and theory of Refs. [47, 48]. It is seen that our approach provides a better agreement with the experiment.

We conclude that the DP model is suitable for calculation of the radial matrix elements and photoionization cross-sections with an accuracy better than a factor of two for low n and much enhanced for higher excited states, as confirmed by the good agreement between experiment and theory in recent lifetime measurements [28, 29].

III. MAPS OF THE COOPER MINIMA

Using the quasiclassical model of Delone et al. [42], in Ref. [11] it has been shown that the radial matrix elements for bound-bound, bound-free and free-free transitions could be expressed in a universal way through the numerically calculated relative matrix elements R_{rel} , multiplied by the appropriate normalization factors:

$$\begin{aligned}
R(nL \rightarrow n'L') &= \frac{0.4108 \times R_{rel}(E_n L \rightarrow E_{n'} L')}{n_{eff}'^{3/2} \times n_{eff}^{3/2} \times |E_{n'} - E_n|^{5/3}} = \\
&= \frac{0.4108 \times R_{rel}(E_n L \rightarrow E_{n'} L')}{(-2E_{n'})^{-3/4} \times (-2E_n)^{-3/4} \times |E_{n'} - E_n|^{5/3}} \\
R(nL \rightarrow E'L') &= \frac{0.4108 \times R_{rel}(E_n L \rightarrow E'L')}{n_{eff}^{3/2} \times |E' - E_n|^{5/3}} = \\
&= \frac{0.4108 \times R_{rel}(E_n L \rightarrow E'L')}{(-2E_n)^{-3/4} \times |E' - E_n|^{5/3}} \\
R(EL \rightarrow E'L') &= \frac{0.4108 \times R_{rel}(EL \rightarrow E'L')}{|E' - E|^{5/3}} \quad (2)
\end{aligned}$$

The prefactor $(4/3)^{1/3}/\Gamma(1/3) = 0.4108$ results from the asymptotic expression for the quasiclassical matrix elements for $n \rightarrow n+1$ transitions [11]. Relative matrix elements $R_{rel}(EL \rightarrow E'L')$ introduced in Eq.(2) are convenient as these are slowly varying functions of E and E' . The dependence of $R_{rel}(EL \rightarrow E'L')$ on the energy E' of the final state passes smoothly through the ionization threshold [11]. The asymptotic $|E' - E|^{-5/3}$ dependence of the radial matrix elements is incorrect for transitions between neighboring states with $E \approx E'$, where the dipole matrix elements rapidly increase [11]. In this case the radial matrix elements can be calculated numerically using a DP model [33, 34], or NCA [36].

We have calculated the relative matrix elements $R_{rel}(E_n L \rightarrow E_{n'} L')$, $R_{rel}(E_n L \rightarrow E'L')$, $R_{rel}(EL \rightarrow E'L)$ for transitions between S , P , D and F states of alkali-metal atoms, starting from the ground state. The energies of the continuum states were taken within $0 < E < 0.5$ (atomic units) to extend the results of Ref. [11] to the area where Cooper minima are expected for alkali-metal atoms.

A. Rubidium

Rubidium and cesium atoms are widely employed in laser cooling experiments, and we shall discuss them in more detail. The relative matrix elements $R_{rel}(S_{1/2} \rightarrow P_{1/2})$ for rubidium are shown in Fig. 4. Following Ref. [11], we present our numerical results as density plots. We use both E -scaled and n -scaled plots, since the latter are more appropriate to the relative matrix elements for bound-bound and bound-free transitions from states with large principal quantum numbers n . The signs of the radial matrix elements are unimportant in the calculation of transition probabilities and photoionization cross-sections, therefore we present only their absolute values.

Figure 4(a) shows the relative matrix elements $R_{rel}(nS_{1/2} \rightarrow E'P_{1/2})$ for bound-free transitions in rubidium atoms. The horizontal axis is the principal quantum number of the nS states, while the vertical axis

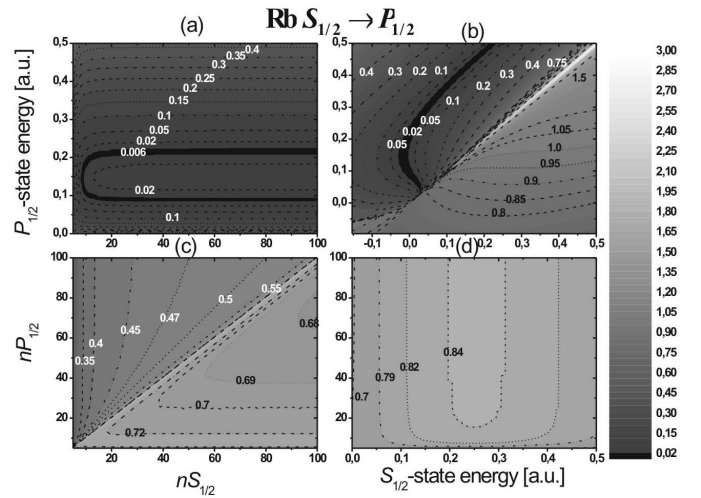


FIG. 4. (Color online). Density plots of the relative matrix elements for (a) Rb bound-free $nS_{1/2} \rightarrow E'P_{1/2}$ transitions; (b) arbitrary Rb $ES_{1/2} \rightarrow E'P_{1/2}$ transitions including discrete and continuum spectra; (c) Rb bound-bound $nS_{1/2} \rightarrow n'P_{1/2}$ transitions; (d) Rb bound-free $nP_{1/2} \rightarrow E'S_{1/2}$ transitions.

is the binding energy E' of the continuum P states (in atomic units). From Fig. 4(a) one finds that for a bound-free transition between the Rydberg $40S_{1/2}$ state and the continuum $E'P_{1/2}$ state with $E' = 0.18$ the relative matrix element is $R_{rel}(nS_{1/2} \rightarrow E'P_{1/2}) = 0.02$. According to Eq.(1) and Table 1 in the appendix A the energy of the $40S_{1/2}$ state is $E_n = -3.68 \times 10^{-4}$, and the energy difference is $|E' - E_n| = 0.18$. Then the absolute radial matrix element can be found from Eq.(2): $R(40S_{1/2} \rightarrow E'P_{1/2}) = 6.1 \times 10^{-4}$. To highlight Cooper minima, the regions where the relative matrix element $R_{rel}(nS_{1/2} \rightarrow E'P_{1/2})$ falls below 0.02 are filled by black. The interesting feature of Fig. 4(a) is the presence of the two sharp Cooper minima at $E' = 0.09$ and $E' = 0.21$ for $n > 10$.

Figure 4(b) shows the relative matrix elements for all possible bound-bound, bound-free and free-free $R_{rel}(S_{1/2} \rightarrow P_{1/2})$ transitions in rubidium atoms, plotted in the energy scale. The horizontal axis carries the binding energy of S states while the binding energy of P states is given in the vertical axis. For a bound-free transition between the $6P_{1/2}$ state with $E = -0.045$ and the continuum $S_{1/2}$ state with $E' = 0.15$, the relative matrix element is $R_{rel}(E_n P_{1/2} \rightarrow E'S_{1/2}) = 0.8$. Then Eq. (2) gives the absolute radial matrix element $R(E_n P_{1/2} \rightarrow E'S_{1/2}) = 0.82$ (the energy difference is $|E' - E| = 0.195$). The same procedure can be applied to calculate radial matrix elements for all bound-bound, bound-free and free-free transitions.

A prominent Cooper minimum is observed in Fig. 4(a), (b) for the bound-free $nS_{1/2} \rightarrow E'P_{1/2}$ and free-free $ES_{1/2} \rightarrow E'P_{1/2}$ transitions in rubidium. For the $nS_{1/2}$ states with $E_n > -0.03$ (corresponding to

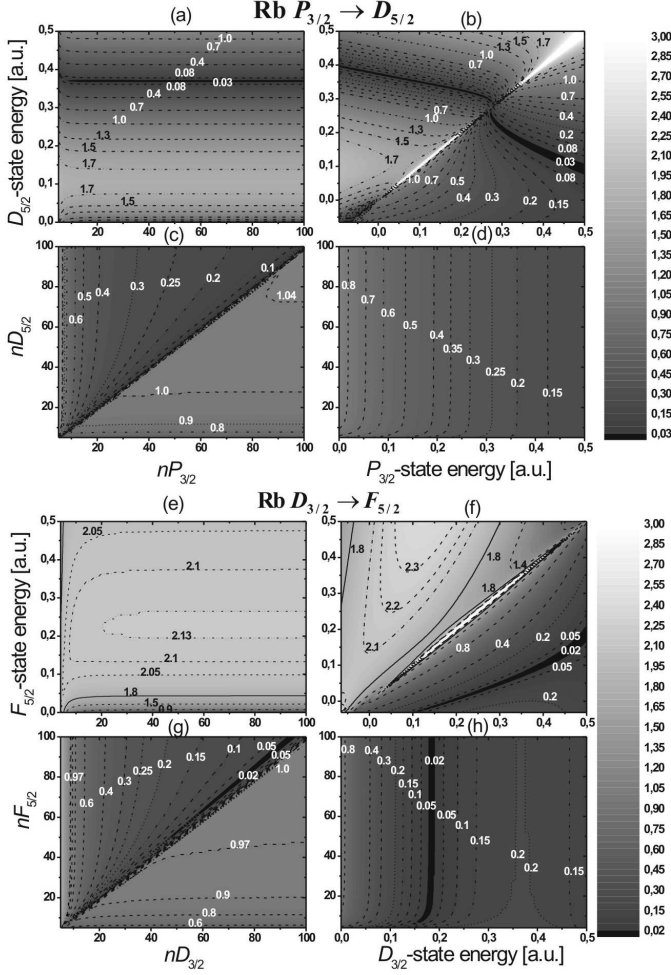


FIG. 5. (Color online). Density plots of the relative matrix elements in Rb atoms for (a) bound-free $nP_{3/2} \rightarrow E'D_{5/2}$ transitions; (b) all $EP_{3/2} \rightarrow E'D_{5/2}$ transitions; (c) bound-bound $nP_{3/2} \rightarrow n'D_{5/2}$ transitions; (d) bound-free $nD_{5/2} \rightarrow E'P_{3/2}$ transitions; (e) bound-free $nD_{3/2} \rightarrow E'F_{5/2}$ transitions; (f) all $ED_{3/2} \rightarrow E'F_{5/2}$ transitions; (g) bound-bound $nD_{3/2} \rightarrow n'F_{5/2}$ transitions; (h) bound-free $nF_{5/2} \rightarrow E'D_{3/2}$ transitions.

$n > 7$) the relative matrix elements fall down below 0.02, while for the lower $nS_{1/2}$ states the minimum is not so sharp.

The relative matrix elements $R_{rel}(E_n P_{1/2} \rightarrow E_n' S_{1/2})$ for bound-bound transitions in rubidium are presented in Fig. 4(c). Since the relative matrix elements slowly vary with n and n' , accurate calculation of the radial matrix elements from the data of Fig. 4(c) is possible as described earlier. For example, $R_{rel}(27S_{1/2} \rightarrow 80P_{1/2}) = 0.45$, $E_{27S} = -8.776 \times 10^{-4}$, $E_{80P} = -8.36 \times 10^{-5}$ and the energy difference is $|E_{n'} - E_n| = 7.94 \times 10^{-4}$. From Eq. (2) one finds $R(27S_{1/2} \rightarrow 80P_{1/2}) = 0.342$.

Relative matrix elements $R_{rel}(nP_{1/2} \rightarrow E'S_{1/2})$ for bound-free transitions in rubidium atoms are shown in Fig. 4(d). As an example, the relative matrix element

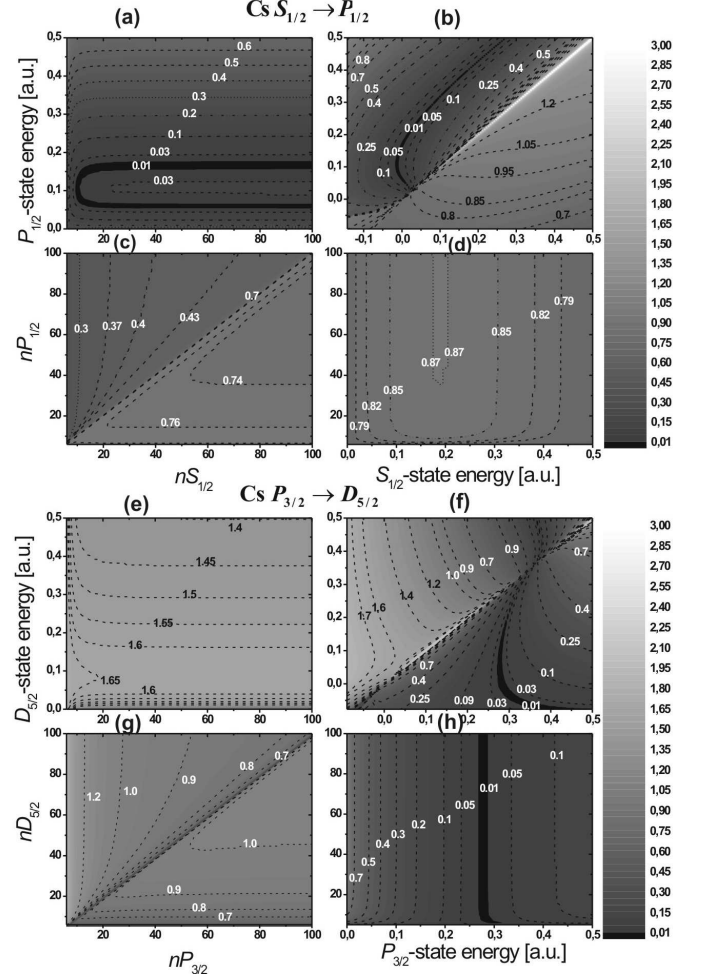


FIG. 6. (Color online). Density plots of the relative matrix elements in Cs atoms for (a) bound-free $nS_{1/2} \rightarrow E'P_{1/2}$ transitions; (b) all $ES_{1/2} \rightarrow E'P_{1/2}$ transitions; (c) bound-bound $nS_{1/2} \rightarrow n'P_{1/2}$ transitions; (d) bound-free $nP_{1/2} \rightarrow E'S_{1/2}$ transitions; (e) bound-free $nP_{3/2} \rightarrow E'D_{5/2}$ transitions; (f) all $EP_{3/2} \rightarrow E'D_{5/2}$ transitions; (g) bound-bound $nP_{3/2} \rightarrow n'D_{5/2}$ transitions; (h) bound-free $nD_{5/2} \rightarrow E'P_{3/2}$ transitions.

is $R_{rel}(60P_{1/2} \rightarrow E'S_{1/2}) = 0.84$ for $E' = 0.2$; then the radial matrix element is $R(60P_{1/2} \rightarrow E'S_{1/2}) = 0.012$.

Figure 5 displays the relative matrix elements $R_{rel}(P_{3/2} \rightarrow D_{5/2})$ and $R_{rel}(D_{3/2} \rightarrow F_{5/2})$ for rubidium atoms in the same way as in Fig. 4. Relative matrix elements for other fine-structure components of the rubidium P and D states are not presented, since the difference between them is too small to be distinguishable on our density plots. Cooper minima are observed for bound-free $nP_{3/2} \rightarrow E'D_{5/2}$ transitions with $E' \approx 0.37$ [Fig. 5(a)], free-free $EP_{3/2} \rightarrow E'D_{5/2}$ and $ED_{3/2} \rightarrow F_{5/2}$ transitions [Fig. 5(b)], and bound-free $nF_{5/2} \rightarrow E'D_{3/2}$ transitions with $E' \approx 0.17$ [Fig. 5(h)].

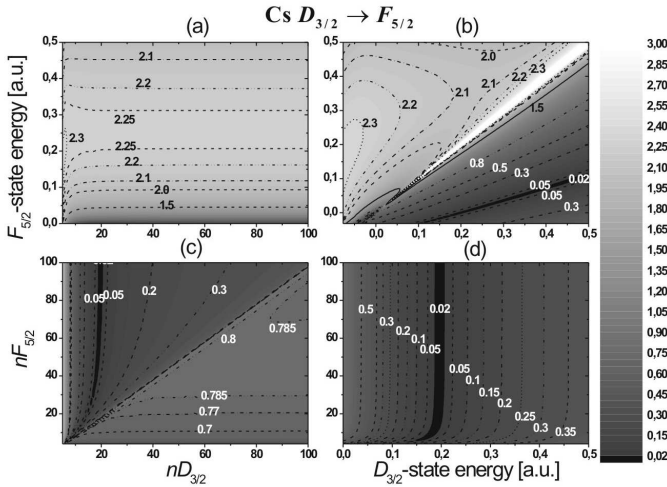


FIG. 7. (Color online). Density plots of the relative matrix elements in Cs atoms for (a) bound-free $nD_{3/2} \rightarrow E'F_{5/2}$ transitions; (b) all $ED_{3/2} \rightarrow E'F_{5/2}$ transitions; (c) bound-bound $nD_{3/2} \rightarrow n'F_{5/2}$ transitions; (d) bound-free $nF_{5/2} \rightarrow E'D_{3/2}$ transitions.

B. Cesium

Figure 6 shows relative matrix elements $R_{rel}(S_{1/2} \rightarrow P_{3/2})$ and $R_{rel}(P_{3/2} \rightarrow D_{5/2})$ for cesium atoms. Relative matrix elements $R_{rel}(D_{3/2} \rightarrow F_{5/2})$ for cesium atoms are presented in Fig. 7. Two Cooper minima are observed for bound-free $nS_{1/2} \rightarrow E'P_{1/2}$ transitions with $E' \approx 0.06$ and $E' \approx 0.17$ in Fig. 6(a). The Cooper minima are also noticed for the bound-free $nD_{5/2} \rightarrow EP_{3/2}$ transitions with $E' \approx 0.28$ [Fig. 6(h)], bound-free $nF_{5/2} \rightarrow E'D_{3/2}$ transitions with $E' = 0.19$ [Fig. 7(h)], and bound-bound $nD_{3/2} \rightarrow n'F_{5/2}$ transitions with $n < 23$ [Fig. 7(g)].

Cooper minimum in the discrete spectrum was first discussed in Ref. [6]. In Ref. [11] a continuation of this minimum in the bound-free $nD_{3/2} \rightarrow E'F_{5/2}$ transitions was found, with the energy $E' \approx 10^{-3}$ being close to the ionization threshold. These features were reproduced in our calculations, but they are not shown due to the large energy scale of our density plots. The near-threshold Cooper minima for Rydberg states of alkali-metal atoms were also discussed in Ref. [11].

C. Lithium

For lithium atoms the relative matrix elements obtained for $R_{rel}(S \rightarrow P)$ and $R_{rel}(P \rightarrow D)$ transitions are shown in Fig. 8, and for $R_{rel}(D \rightarrow F)$ transitions in Fig. 9. Fine structure is neglected due to the small fine splitting. One may see that the matrix elements of the bound-free $S \rightarrow P$ transitions slowly decrease as the energy of the continuum state grows. A Cooper minimum is observed for the bound-bound $nS_{1/2} \rightarrow n'P_{1/2}$

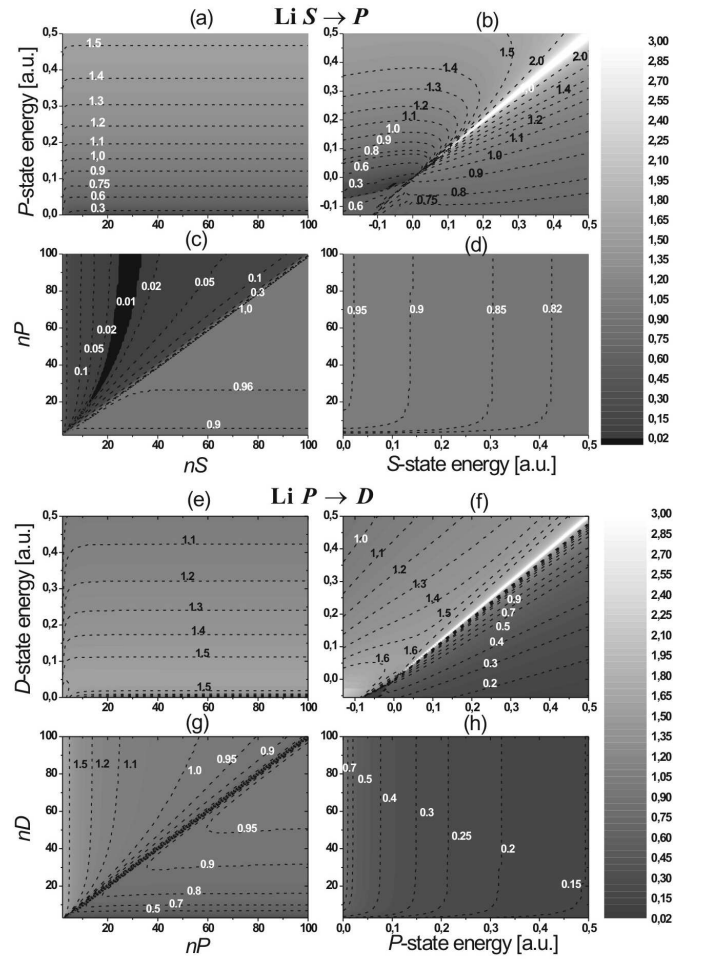


FIG. 8. (Color online). Density plots of the relative matrix elements in Li atoms for (a) bound-free $nS \rightarrow E'P$ transitions; (b) all $ES \rightarrow E'P$ transitions; (c) bound-bound $nS \rightarrow n'P$ transitions; (d) bound-free $nP \rightarrow E'S$ transitions; (e) bound-free $nP \rightarrow E'D$ transitions; (f) all $EP \rightarrow E'D$ transitions; (g) bound-bound $nP \rightarrow n'D$ transitions; (h) bound-free $nD \rightarrow E'P$ transitions.

transitions [Fig. 8(a)]. This minimum has been found earlier in Ref. [10] in an experimental study of the far-infrared transitions between Rydberg states. Later on we have shown that such minimum can also appear in the BBR-induced transitions [50].

D. Sodium

For sodium atoms the relative matrix elements obtained for $R_{rel}(S_{1/2} \rightarrow P_{1/2})$ and $R_{rel}(P_{3/2} \rightarrow D_{5/2})$ transitions are shown in Fig. 10, and for $R_{rel}(D_{3/2} \rightarrow F_{5/2})$ transitions in Fig. 11. A Cooper minimum is observed for the bound-free $nS_{1/2} \rightarrow E'P_{1/2}$ transitions at $E' \approx 0.06$ [Fig. 10(a)], bound-free $nD_{5/2} \rightarrow E'P_{3/2}$ transitions at $E' \approx 0.05$ [Fig. 10(h)], bound-free $nP_{3/2} \rightarrow E'D_{5/2}$ transitions at $E' \approx 0.25$

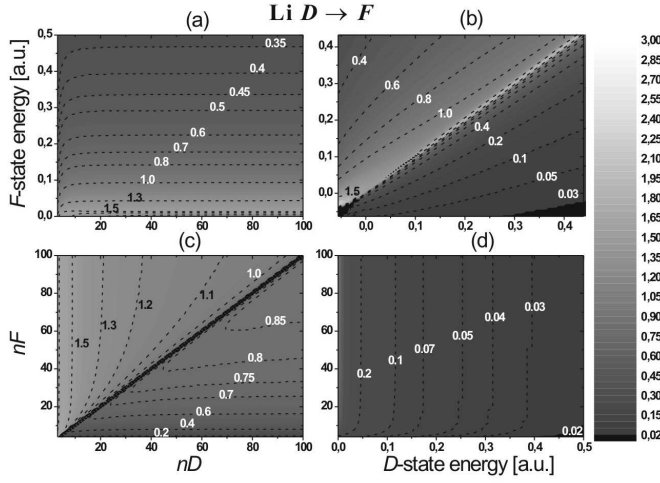


FIG. 9. (Color online). Density plots of the relative matrix elements in Li atoms for (a) bound-free $nD \rightarrow E'F$ transitions; (b) all $ED \rightarrow E'F$ transitions; (c) bound-bound $nD \rightarrow n'F$ transitions; (d) bound-free $nF \rightarrow E'D$ transitions.

[Fig. 10(e)], and bound-free $nF_{5/2} \rightarrow E'D_{3/2}$ transitions at $E' \approx 0.29$ [Fig. 11(d)]. For $nS_{1/2} \rightarrow E'P_{1/2}$ and $nD_{5/2} \rightarrow E'P_{3/2}$ transitions in sodium a Cooper minimum is found to be close to the ionization threshold.

E. Potassium

For potassium atoms the relative matrix elements obtained for $R_{rel}(S_{1/2} \rightarrow P_{1/2})$ and $R_{rel}(P_{3/2} \rightarrow D_{5/2})$ transitions are shown in Fig. 12, and for $R_{rel}(D_{3/2} \rightarrow F_{5/2})$ transitions in Fig. 13. Interesting features are observed in the radial matrix elements of bound-bound and bound-free transitions. The two minima have been located in the relative matrix elements of the bound-free $nS_{1/2} \rightarrow E'P_{1/2}$ transitions at $E' \approx 0.05$ and $E' \approx 0.45$ [Fig. 12(a)]. A Cooper minimum is also observed for $nP_{3/2} \rightarrow E'D_{5/2}$ transitions at $E' \approx 0.29$ [Fig. 12(g)]. A minimum in the discrete spectrum has been found [Fig. 12(c)], which is similar to the lithium $S \rightarrow P$ and cesium $D \rightarrow F$ transitions. This minimum in potassium atoms was first discussed by Theodosiou [6]. Finally, for the bound-free $nF_{5/2} \rightarrow E'D_{3/2}$ transitions in potassium, a Cooper minimum is registered at $E' \approx 0.18$ and $E' \approx 0.38$ [Fig. 13(d)].

IV. CONCLUSION

The quasiclassical model developed by Dyachkov and Pankratov [33, 34] can be used for fast and reliable calculations of the radial matrix elements for bound-bound, bound-free and free-free transitions between arbitrary states of alkali-metal atoms. We have demonstrated this

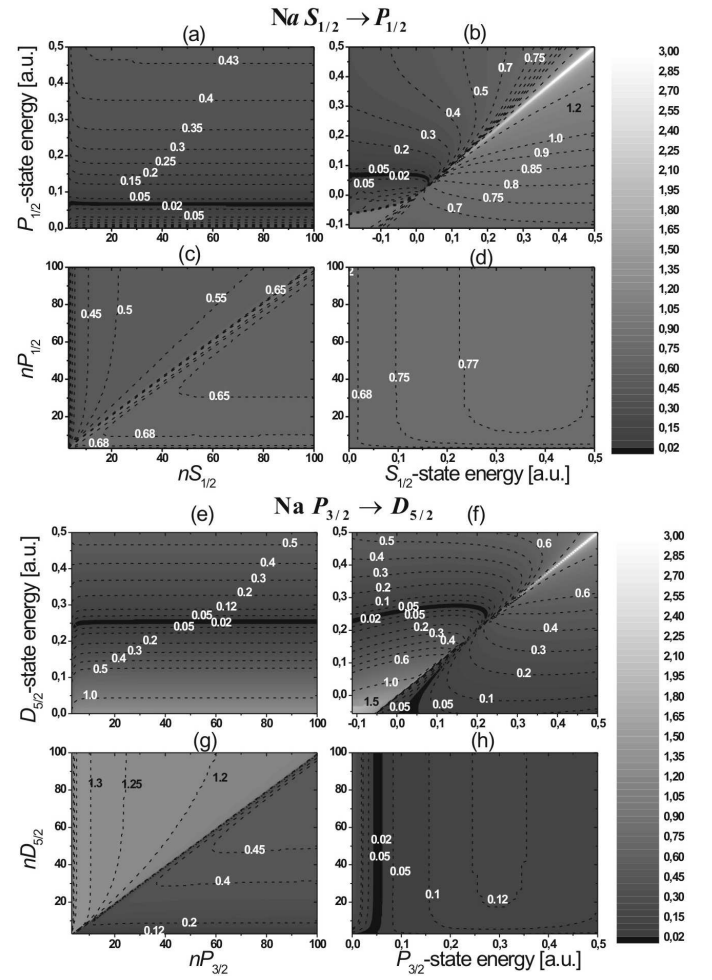


FIG. 10. (Color online). Density plots of the relative matrix elements in Na atoms for (a) bound-free $nS_{1/2} \rightarrow E'P_{1/2}$ transitions; (b) all $ES_{1/2} \rightarrow E'P_{1/2}$ transitions; (c) bound-bound $nS_{1/2} \rightarrow n'P_{1/2}$ transitions; (d) bound-free $nP_{1/2} \rightarrow E'S_{1/2}$ transitions; (e) bound-free $nP_{3/2} \rightarrow E'D_{5/2}$ transitions; (f) all $EP_{3/2} \rightarrow E'D_{5/2}$ transitions; (g) bound-bound $nP_{3/2} \rightarrow n'D_{5/2}$ transitions; (h) bound-free $nD_{5/2} \rightarrow E'P_{3/2}$ transitions.

by performing the numerical calculations of the radial matrix elements for transitions between S , P , D and F states with the energies $E < 0.5$ (in atomic units) in all alkali-metal atoms. Our results on radial matrix elements are in good agreement with numerical calculations in the Coulomb approximations [11]. Our theoretical results [14] are also consistent with the experimental measurements of the effective lifetimes of Rydberg states [28, 29], oscillator strengths [22, 23], and photoionization cross-sections [7]. Our approach allowed us to reveal several unknown Cooper minima, both in the discrete and continuum spectra, which would be interesting to confirm experimentally. Reliability of the quasiclassical model for study of the Cooper minima is verified by good agreement with calculations of Ref. [6] for bound-bound transitions and satisfactory agreement with calcu-

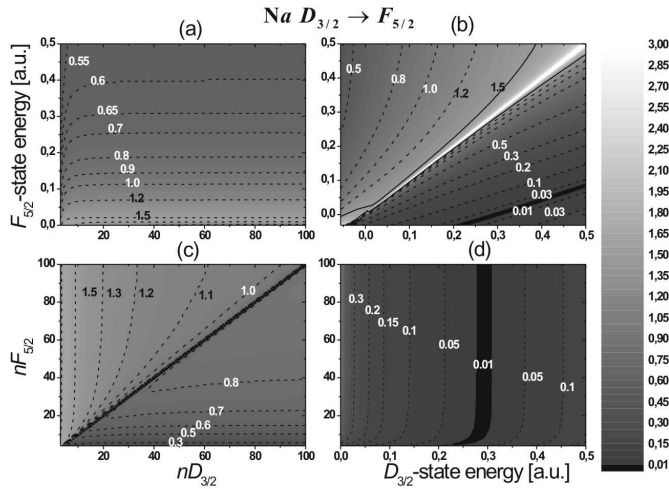


FIG. 11. (Color online). Density plots of the relative matrix elements in Na atoms for (a) bound-free $nD_{3/2} \rightarrow E'F_{5/2}$ transitions; (b) all $ED_{3/2} \rightarrow E'F_{5/2}$ transitions; (c) bound-bound $nD_{3/2} \rightarrow n'F_{5/2}$ transitions; (d) bound-free $nF_{5/2} \rightarrow E'D_{3/2}$ transitions;

lations of Ref. [8] for bound-free transitions. We conclude that the quasiclassical model of Dyachkov and Pankratov is a universal method for systematic calculation of the radial matrix elements for transitions between excited states of alkali-metal atoms.

V. ACKNOWLEDGMENTS

This work was supported by Grants of the President of Russia MK.7060.2012.2, MK.3727.2011.2, RFBR Grant No. 10-02-00133, Russian Academy of Sciences and the Dynasty foundation. SB, CM, AK and CMC acknowledge support from EPSRC grant No. EP/F031130/1.

Appendix A: The quantum defects.

The values of the quantum defect can be obtained by fitting the experimentally measured energies to Eq.(1) [51]:

$$\mu_L(n) = a'_L + \frac{b'_L}{n_{eff}^2} + \frac{c'_L}{n_{eff}^4} + \frac{d'_L}{n_{eff}^6} + \frac{e'_L}{n_{eff}^8} \dots, \quad (\text{A1})$$

where a'_L , b'_L , c'_L , d'_L , e'_L are the Rydberg-Ritz fitting coefficients. The quantum defects can also be expressed through the modified Rydberg-Ritz coefficients, which were tabulated for alkali-metal Rydberg atoms in Ref. [51]:

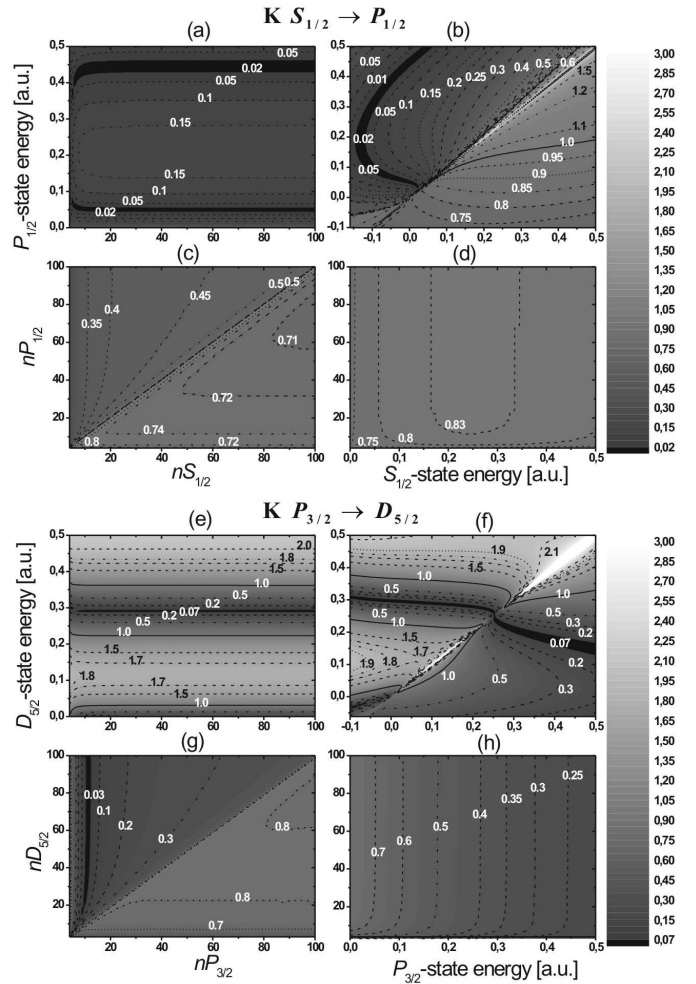


FIG. 12. (Color online). Density plots of the relative matrix elements in K atoms for (a) bound-free $nS_{1/2} \rightarrow E'P_{1/2}$ transitions; (b) all $ES_{1/2} \rightarrow E'P_{1/2}$ transitions; (c) bound-bound $nS_{1/2} \rightarrow n'P_{1/2}$ transitions; (d) bound-free $nP_{1/2} \rightarrow E'S_{1/2}$ transitions; (e) bound-free $nP_{3/2} \rightarrow E'D_{5/2}$ transitions; (f) all $EP_{3/2} \rightarrow E'D_{5/2}$ transitions; (g) bound-bound $nP_{3/2} \rightarrow n'D_{5/2}$ transitions; (h) bound-free $nD_{5/2} \rightarrow E'P_{3/2}$ transitions.

$$\mu_L(n) = a_L + \frac{b_L}{(n - a_L)^2} + \frac{c_L}{(n - a_L)^4} + \frac{d_L}{(n - a_L)^6} + \frac{e_L}{(n - a_L)^8} \dots \quad (\text{A2})$$

The difference between the fitting coefficients in Eqs.(A1) and (A2) is small and lies within the measurement uncertainty [51]. The most recent experimental values of the modified Rydberg-Ritz coefficients [57] available for alkali-metal Rydberg atoms are listed in Table 1 of Appendix. The data are taken from Refs. [51–57].

We have compared our calculations with our recent experimental data for diffuse series in rubidium. Good agreement between experiment and theory is observed.

TABLE I. Quantum defects of alkali-metal Rydberg states

		$S_{1/2}$	$P_{1/2}$	$P_{3/2}$	$D_{3/2}$	$D_{5/2}$	$F_{5/2}$ $F_{7/2}$
Li [52]	a	0.39951183	0.04716876		0.00194211		0.00030862
	b	0.02824560	-0.02398188		-0.00376875		-0.00099057
	c	0.02082123	0.01548488		-0.01563348		-0.00739661
	d	-0.09793152	-0.16065777		0.10335313		
	e	0.14782202	0.33704280				
Na [53]	a	1.34796938(11)	0.85544502(15)	0.85462615(12)	0.014909286(97)	0.01492422(16)	0.001453*
	b	0.060989(16)	0.112067(86)	0.112344(67)	-0.042506(35)	-0.042585(43)	0.017312*
	c	0.019674(17)	0.0479(13)	0.0497(10)	0.00840(31)	0.00840(39)	-0.7809*
	d	-0.001045(354)	0.0457(43)	0.0406(34)			7.021*
K [51]	a	2.1801985	1.713892	1.710848	0.276970	0.2771580	0.010098
	b	0.13558	0.233294	0.235437	-1.024911	-1.025635	-0.100224
	c	0.0759	0.16137	0.11551	-0.709174	-0.59201	1.56334
	d	0.117	0.5345	1.1015	11.839	10.0053	-12.6851
	e	-0.206	-0.234	-2.0356	-26.689	-19.0244	
Rb [54, 55]	a	3.1311804(10)	2.6548849(10)	2.6416737(10)	1.34809171(40)	1.34646572(30)	0.0165192(9) ($F_{5/2}$)
							0.0165437(7) ($F_{7/2}$)
		0.1784(6)	0.2900(6)	0.2950(7)	-0.60286(26)	-0.59600(18)	-0.085(9) ($F_{5/2}$) -0.086(7) ($F_{7/2}$)
Cs [56]	a	4.04935665(38)	3.59158950(58)	3.5589599**	2.4754562**	2.46631524(63)	0.03341424(96)
	b	0.2377037	0.360926	0.392469**	0.009320**	0.013577	-0.198674
	c	0.255401	0.41905	-0.67431**	-0.43498**	-0.37457	0.28953
	d	0.00378	0.64388	22.3531**	-0.76358**	-2.1867	-0.2601
	e	0.25486	1.45035	-92.289**	-18.0061**	-1.5532	

*[51]

**[57]

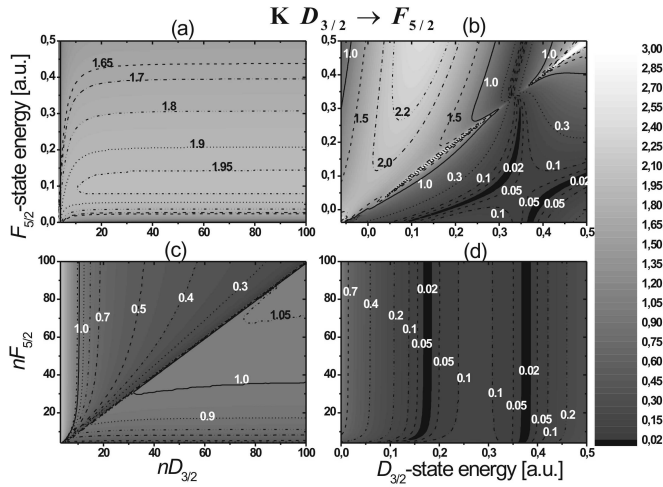


FIG. 13. (Color online). Density plots of the relative matrix elements in K atoms for (a) bound-free $nD_{3/2} \rightarrow E'F_{5/2}$ transitions; (b) all $ED_{3/2} \rightarrow E'F_{5/2}$ transitions; (c) bound-bound $nD_{3/2} \rightarrow n'F_{5/2}$ transitions; (d) bound-free $nF_{5/2} \rightarrow E'D_{3/2}$ transitions.

For the calculation of the dipole matrix elements of bound-free and free-free transitions, the expressions for the quantum defects of Rydberg states, given by

Eqs.(A1) and (A2), must be extrapolated to the continuum [58]:

$$\mu_L(E) = a_L + b_L \times (-2E) + c_L \times (-2E)^2 + d_L \times (-2E)^3 \dots \quad (\text{A3})$$

Here E is energy of the continuum state. We have found that calculations of the radial matrix elements for bound-free and free-free transitions are sensitive to the way of extrapolation of the quantum defects into continuum, especially in the regions of the Cooper minima. This was also discussed earlier in Ref. [49]. The most recent data for the rubidium quantum defects [54, 55] contain only two coefficients a_L and b_L , while for the other alkali-metal atoms up to five terms of Eq.(A2) have been published [51–53, 56, 57]. However, our test for using the higher-order polynomial approximations gave incorrect values of the quantum defects at large energies of the continuum states, due to the well known Runge's phenomenon [59] of oscillation of the interpolation function near the edge of the interpolation region, when the higher-order polynomial approximation is used. Therefore, in our calculations we applied a linear extrapolation of quantum defects to the continuum with only the first two terms of Eq. (A3).

Appendix B: Dyachkov-Pankratov quasiclassical model

A quasiclassical model of Dyachkov and Pankratov was published in their original papers [33, 34]. Here we summarize the main formulas, which are used to calculate the relative matrix elements for bound-bound, bound-free and free-free transitions between $|E, L\rangle$ and $|E', L'\rangle$ states and transition frequency $\omega = E' - E$, where $E' > E$. The difference of the quantum defects $\Delta\mu = \mu_{L'}(E') - \mu_L(E)$.

The Kepler motion of quasiclassical electron is determined by the mean energy:

$$E_c = \frac{E + E'}{2}. \quad (\text{B1})$$

The cases of $E_c < 0$ (finite mean orbit) and $E_c > 0$ (infinite mean orbit) must be considered separately. If $E_c < 0$ (bound-bound transitions and bound-free transitions to the continuum states with $E' < |E|$), the parameters γ^* , γ and mean quantum number ν_c are defined as:

$$\begin{aligned} \gamma^* &= \frac{\omega}{|E + E'|^{3/2}}, \\ \gamma &= \text{int}[\gamma^* + \Delta\mu + 0.5] - \Delta\mu, \\ \nu_c &= (\gamma/\omega)^{1/3}. \end{aligned} \quad (\text{B2})$$

Here $\text{int}[x]$ means integer part of x . In the quasiclassical model the dynamics of the electron is defined by the arithmetic mean orbital momentum l_c and eccentricity of the mean elliptic orbit of the electron ε :

$$l_c = \frac{L + L' + 1}{2}, \quad \varepsilon = \left(1 - \frac{l_c^2}{\nu_c^2}\right)^{1/2}. \quad (\text{B3})$$

The relative matrix element is then expressed as:

$$\begin{aligned} R_{rel}(EL \rightarrow E'L') &= \frac{\nu_c^2 \omega^{2/3}}{0.4108} [U_\gamma(\varepsilon\gamma) \cos(\pi\Delta\mu) - V_\gamma(\varepsilon\gamma) \sin(\pi\Delta\mu)], \\ U_\gamma &= J'_\gamma(\varepsilon\gamma) + \Delta l \frac{l_c}{\nu_c \varepsilon} J_\gamma(\varepsilon\gamma), \\ V_\gamma &= E'_\gamma(\varepsilon\gamma) + \Delta l \frac{l_c}{\nu_c \varepsilon} \left[E_\gamma(\varepsilon\gamma) - \frac{1}{\pi\gamma} \right] + \frac{1 - \varepsilon}{\pi}. \end{aligned} \quad (\text{B4})$$

Here J_γ and E_γ are the Anger and Weber functions, respectively, J'_γ and E'_γ are their derivatives with respect to argument.

If $E_c > 0$ (bound-free transitions with $E' > |E|$ and free-free transitions), the relative matrix element is given by:

$$\begin{aligned} R_{rel}(EL \rightarrow E'L') &= \frac{\eta_c^2 \omega^{2/3}}{0.4108} [P_\gamma(\varepsilon\gamma) \cos(\pi\Delta\mu) - Q_\gamma(\varepsilon\gamma) \sin(\pi\Delta\mu)], \\ P_\gamma &= -g'_\gamma(\varepsilon\gamma) + \Delta l \frac{l_c}{\eta_c \varepsilon} g_\gamma(\varepsilon\gamma), \\ Q_\gamma &= h'_\gamma(\varepsilon\gamma) + \Delta l \frac{l_c}{\eta_c \varepsilon} \left[h_\gamma(\varepsilon\gamma) - \frac{1}{\pi\gamma} \right] + \frac{\varepsilon - 1}{\pi}. \end{aligned} \quad (\text{B5})$$

Here $\eta_c = 1/\sqrt{2E_c}$, $\gamma = \eta_c^3 \omega$ and $\varepsilon = (1 + l_c^2/\eta_c^2)^{1/2}$.

Functions g_γ and h_γ are expressed through the Hankel $H^{(1)}$, Anger J and modified Bessel I functions:

$$\begin{aligned} g_\gamma(y) &= \frac{1}{2} i H_{i\gamma}^{(1)}(iy), \\ h_\gamma(y) &= \frac{1}{\sinh(\pi\gamma)} \left\{ J_{i\gamma}(-iy) - \frac{1}{2} \exp(\pi\gamma/2) [I_{iy}(\gamma) + I_{-iy}(\gamma)] \right\} \end{aligned} \quad (\text{B6})$$

In the case of $E_c \approx 0$ an asymptotic expression for relative matrix element can be used:

$$R_{rel}(EL \rightarrow E'L') = \frac{4^{1/3}}{0.4108} \{[S(x) + \beta S_1(x)] \cos(\pi\Delta\mu) - [T(x) + \beta T_1(x)] \sin(\pi\Delta\mu)\} \quad (\text{B7})$$

Here $x = (l_c^3\omega/2)^{2/3}$, $\beta = 2E_c(2/\omega)^{2/3}$, and functions $S(x)$, $S_1(x)$, $T(x)$, $T_1(x)$ are expressed through the Airy $Ai(x)$ and $Bi(x)$ functions, their derivatives and hypergeometric function ${}_1F^2$:

$$\begin{aligned} S(x) &= \Delta l \cdot x^{1/2} \cdot Ai(x) - Ai'(x), \\ T(x) &= \Delta l \cdot x^{1/2} \cdot Gi(x) - Gi'(x) + \frac{x}{2\pi}, \\ S_1(x) &= \frac{1}{10} \left(1 - 6\Delta l \cdot x^{3/2} + 4x^3\right) Ai(x) + \frac{2}{5}x \left(1 - \Delta l \cdot x^{3/2}\right) Ai'(x), \\ T_1(x) &= \frac{1}{10} \left(1 - 6\Delta l \cdot x^{3/2} + 4x^3\right) Gi(x) + \frac{2}{5}x \left(1 - \Delta l \cdot x^{3/2}\right) Gi'(x) + \frac{9}{20\pi}\Delta l \cdot x^{1/2} - \frac{21}{40\pi}x^2, \\ Gi(x) &= \frac{1}{3}Bi(x) - \frac{x^2}{2\pi}{}_1F^2\left(1; \frac{4}{3}, \frac{5}{3}; \frac{x^3}{3}\right), \\ Gi'(x) &= \frac{Bi(x)}{3} - \frac{x}{\pi}{}_1F^2\left(1; \frac{4}{3}, \frac{5}{3}; \frac{x^3}{9}\right) - \frac{3x^4}{40\pi}{}_1F^2\left(2; \frac{7}{3}, \frac{8}{3}; \frac{x^3}{9}\right) + \frac{x}{2\pi}. \end{aligned} \quad (\text{B8})$$

We note that in the original paper [33] there were misprints in the last two terms in the expression for $T_1(x)$. Here we present the corrected formula kindly provided by L. G. Dyachkov [60].

To simplify numerical calculations with generic mathematical codes and software, functions J_γ , E_γ , g_γ , h_γ and their derivatives can be expressed via more commonly used regularized hypergeometric functions ${}_1\tilde{F}^2$, hypergeometric functions ${}_1F^2$, Hankel H and modified Bessel I functions [61]:

$$\begin{aligned} J_\gamma(z) &= \frac{1}{2}z \sin\left(\frac{\pi\gamma}{2}\right) {}_1\tilde{F}^2\left[1; \frac{1}{2}(3-\gamma), \frac{1}{2}(3+\gamma); -\frac{z^2}{4}\right] + \cos\left(\frac{\pi\gamma}{2}\right) {}_1\tilde{F}^2\left[1; 1 - \frac{\gamma}{2}, 1 + \frac{\gamma}{2}; -\frac{z^2}{4}\right], \\ E_\gamma(z) &= -\frac{1}{2}z \cos\left(\frac{\pi\gamma}{2}\right) {}_1\tilde{F}^2\left[1; \frac{1}{2}(3-\gamma), \frac{1}{2}(3+\gamma); -\frac{z^2}{4}\right] + \sin\left(\frac{\pi\gamma}{2}\right) {}_1\tilde{F}^2\left[1; 1 - \frac{\gamma}{2}, 1 + \frac{\gamma}{2}; -\frac{z^2}{4}\right], \\ J'_\gamma(z) &= -\frac{1}{2}z \cos\left(\frac{\pi\gamma}{2}\right) {}_1\tilde{F}^2\left[2; 2 - \frac{\gamma}{2}, 2 + \frac{\gamma}{2}; -\frac{z^2}{4}\right] + \\ &\quad + \frac{1}{2} \sin\left(\frac{\pi\gamma}{2}\right) {}_1\tilde{F}^2\left[1; \frac{3-\gamma}{2}, \frac{3+\gamma}{2}; -\frac{z^2}{4}\right] - \frac{z^2}{4} \sin\left(\frac{\pi\gamma}{2}\right) {}_1\tilde{F}^2\left[1; 1 + \frac{3-\gamma}{2}, 1 + \frac{3+\gamma}{2}; -\frac{z^2}{4}\right], \\ E'_\gamma(z) &= -\frac{1}{2}z \sin\left(\frac{\pi\gamma}{2}\right) {}_1\tilde{F}^2\left[2; 2 - \frac{\gamma}{2}, 2 + \frac{\gamma}{2}; -\frac{z^2}{4}\right] - \\ &\quad - \frac{1}{2} \cos\left(\frac{\pi\gamma}{2}\right) {}_1\tilde{F}^2\left[1; \frac{3-\gamma}{2}, \frac{3+\gamma}{2}; -\frac{z^2}{4}\right] + \frac{z^2}{4} \cos\left(\frac{\pi\gamma}{2}\right) {}_1\tilde{F}^2\left[1; 1 + \frac{3-\gamma}{2}, 1 + \frac{3+\gamma}{2}; -\frac{z^2}{4}\right]. \\ g'_\gamma(z) &= \frac{1}{4} \left[-H_{-1+i\gamma}^{(1)}(iz) + H_{1+i\gamma}^{(1)}(iz)\right], \\ h'_\gamma(z) &= \cosh(\pi\gamma) \left\{ -\frac{1}{4} \exp\left(\frac{\pi\gamma}{2}\right) [I_{-1-i\gamma}(z) + I_{1-i\gamma}(z) + I_{-1+i\gamma}(z) + I_{1+i\gamma}(z)] \right\} + \\ &\quad + \frac{1}{2}z \cosh\left(\frac{\pi\gamma}{2}\right) {}_1F^2\left(2; 2 - \frac{i\gamma}{2}, 2 + \frac{i\gamma}{2}; \frac{z^2}{4}\right) + \frac{1}{2} \sinh\left(\frac{\pi\gamma}{2}\right) {}_1F^2\left(1; \frac{3-i\gamma}{2}, \frac{3+i\gamma}{2}; \frac{z^2}{4}\right) + \\ &\quad + \frac{z^2}{4} {}_1F^2\left(1; 1 + \frac{3-i\gamma}{2}, 1 + \frac{3+i\gamma}{2}; \frac{z^2}{4}\right). \end{aligned} \quad (\text{B9})$$

[1] D. R. Bates, Proc. R. Soc. Lond. A **188**, 350 (1947).

[2] M. Aymar, J. Phys. B **1279**, 9 (1976).

- [3] J. W. Cooper, Phys. Rev. **128**, 681 (1962).
- [4] U. Fano and J. W. Cooper, Rev. Mod. Phys. **40**, 441 (1968).
- [5] R. W. Ditchburn, J. Tunstead, and J. G. Yates, Proc. R. Soc. Lond. A **181**, 386 (1943).
- [6] C. E. Theodosiou, J. Phys. B **L1**, 13 (1980).
- [7] R. D. Hudson and V. L. Carter, Journ. Opt. Soc. Am. **651**, 57 (1967).
- [8] M. Aymar, J. Phys. B **1413**, 11 (1978).
- [9] A. Z. Msezane and S. T. Manson, Phys. Rev. Lett **473**, 48 (1982).
- [10] J. H. Hoogenraad, R. B. Vrijen, P. W. van Amersfoort, A. F. G. van der Meer, and L. D. Noordam, Phys. Rev. Lett. **75**, 4579 (1995).
- [11] J. H. Hoogenraad and L. D. Noordam, Phys. Rev. A. **57**, 4533 (1998).
- [12] D. I. Duncan, J. deBor, H. G. Muller, and L. D. Noordam, Phys. Rev. A. **56**, 4985 (1997).
- [13] I. D. Petrov, V. L. Sukhorukov, E. L. Eber, and H. Hotop, Eur. Phys. J. D. **10**, 53 (2000).
- [14] I. I. Beterov, I. I. Ryabtsev, D. B. Tretyakov, and V. M. Entin, Phys. Rev. A **79**, 052504 (2009).
- [15] I. I. Beterov, D. B. Tretyakov, I. I. Ryabtsev, A. Ekers, and N. N. Bezuglov, Phys. Rev. A **75**, 052720 (2007).
- [16] I. I. Beterov, D. B. Tretyakov, I. I. Ryabtsev, N. N. Bezuglov, and A. Ekers, New Journal of Physics **11**, 013052 (2009).
- [17] T. Amthor, J. Denskat, C. Giese, N. N. Bezuglov, A. Ekers, L. S. Cederbaum, and M. Weidemuller, Eur. Phys. J. **53**, 329 (2009).
- [18] R. M. Potvliege and C. S. Adams, New Journal of Physics **8**, 163 (2006).
- [19] J. Tallant, D. Booth, and J. P. Shaffer, Phys. Rev. A **82**, 063406 (2010).
- [20] L. Fechner, B. Groner, A. Sieg, C. Callegari, F. Ancilotto, F. Stienkemeier, and M. Mudrich, Phys. Chem. Chem. Phys. **14**, 3843 (2012).
- [21] A. Nadeem and S. U. Haq, Phys. Rev. A **81**, 063432 (2010).
- [22] A. Nadeem and S. U. Haq, Phys. Rev. A **83**, 063404 (2011).
- [23] M. J. Piotrowicz, C. MacCormick, A. Kowalczyk, S. Bergamini, I. I. Beterov, and E. A. Yakshina, New Journal of Physics **13**, 093012 (2011).
- [24] M. Fabry and J. R. Cussenot, Can. J. Phys. **54**, 836 (1976).
- [25] S. Hussain, M. Saleem, and M. A. Baig, Phys. Rev. A **75**, 022710 (2007).
- [26] M. A. Baig, S. Mahmood, M. A. Kalyar, N. Amin, and S. U. Haq, Eur. Phys. J. D **44**, 9 (2007).
- [27] C. Gabbanini, Spectrochimica Acta Part B **61**, 196 (2006).
- [28] Z. G. Feng, L. J. Zhang, J. M. Zhao, C. Y. Li, and S. T. Jia, J. Phys. B **42**, 145303 (2009).
- [29] D. B. Branden, T. Juhasz, T. Machlokozera, C. Vesa, R. O. Wilson, M. Zheng, A. Kortyna, and D. A. Tate, J. Phys. B **43**, 015002 (2010).
- [30] M. Viteau, J. Radogostowicz, A. Chotia, M. G. Bason, N. Malossi, F. Fuso, D. Ciampini, O. Morsch, I. I. Ryabtsev, and E. Arimondo, J. Phys. B **43**, 155301 (2010).
- [31] R. J. Knize, B. V. Zhdanov, and M. K. Shaffer, Optics Express **19**, 7894 (2011).
- [32] S. Zhang, F. Robicheaux, and M. Saffman, Phys. Rev. A **84**, 043408 (2011).
- [33] L. G. Dyachkov and P. M. Pankratov, J. Phys. B **461** (1994).
- [34] L. G. Dyachkov and P. M. Pankratov, Opt. Spectrosc. **68** (1990).
- [35] H. A. Bethe and E. E. Salpeter, *Quantum Mechanics of One- and Two-Electron Atoms* (Springer, Berlin, 1957).
- [36] M. L. Zimmerman, M. G. Littman, M. M. Kash, and D. Kleppner, Phys. Rev. A **20**, 2251 (1979).
- [37] S. Klarsfeld, Phys. Rev. A **39**, 2324 (1989).
- [38] L. A. Bureeva, Astron. J. (USSR) **45**, 1215 (1968).
- [39] P. F. Naccache, J. Phys. B **5**, 1308 (1972).
- [40] A. R. Edmonds, J. Picart, N. T. Minh, and R. Pullen, J. Phys. B **12**, 2781 (1979).
- [41] V. A. Davydkin and B. A. Zon, Opt. Spectrosc. **51**, 13 (1981).
- [42] N. B. Delone, S. P. Goreslavsky, and V. P. Krainov, J. Phys. B **27**, 4403 (1994).
- [43] V. D. Ovsiannikov, I. L. Glukhov, and E. A. Nekipelov, Opt. Spectrosc. **111**, 25 (2011).
- [44] M. Marinescu, H. R. Sadeghpour, and A. Dalgarno, Phys. Rev. A **49**, 982 (1994).
- [45] T. F. Gallagher, *Rydberg Atoms* (Cambridge: Cambridge University Press, 1994).
- [46] J. Migdalek and Y. Kim, J. Phys. B **31**, 1947 (1998).
- [47] S. Sahoo and Y. K. Ho, Physics of Plasmas **13**, 063301 (2006).
- [48] G. Peach, H. E. Saraph, and M. J. Seaton, Physics of Plasmas **21**, 3669 (1988).
- [49] N. N. Bezuglov and V. M. Borodin, Opt. Spectrosc. **86**, 467 (1999).
- [50] I. I. Beterov, I. I. Ryabtsev, D. B. Tretyakov, N. N. Bezuglov, and A. Ekers, JETP **107**, 20 (2008).
- [51] C. J. Lorenzen and K. Niemax, Physica Scripta **27**, 300 (1983).
- [52] G. D. Stevens, C. H. Iu, T. Bergeman, H. J. Metcalf, I. Seipp, K. T. Taylor, and D. Delande, Phys. Rev. A **53**, 1349 (1996).
- [53] S. F. Dyubko, M. N. Efimenko, V. A. Efremov, and S. V. Podnos, Quantum Electronics **25**, 914 (1995).
- [54] W. L. I. Mourachko, M. W. Noel, and T. F. Gallagher, Phys. Rev. A **67**, 052502 (2003).
- [55] J. Han, Y. Jamil, D. V. L. Norum, P. J. Tanner, and T. F. Gallagher, Phys. Rev. A **74**, 054502 (2006).
- [56] K. H. Weber and C. J. Sansonetti, Phys. Rev. A **35**, 4650 (1987).
- [57] C. J. Lorenzen and K. Niemax, Z. Phys. A **315**, 127 (1984).
- [58] A. Burgess and M. J. Seaton, Rev. Mod. Phys. **30**, 992 (1958).
- [59] C. Runge, Zeitschrift fur Mathematik und Physik **46**, 224 (1901).
- [60] L. G. Dyachkov, Private communication (2005).
- [61] M. Abramowitz and I. Stegun, *Handbook on Mathematical Functions*, 1st ed. (Dover, New York, 1965).